Results in Physics 10 (2018) 323–331

Contents lists available at ScienceDirect

Results in Physics

journal homepage: www.elsevier.com/locate/rinp

A Monte Carlo study of arms effect in myocardial perfusion of normal and abnormal cases utilizing STL heart shape

Essam Banoqitah[a,*], Eslam Taha[a], Ezzat Elmoujarkach[a], Sahar Alsebaie[b], Ahmad Subahi[c], Shaza Alsharif[c]

[a] Nuclear Engineering Department, King Abdulaziz University, Jeddah, Saudi Arabia
[b] Department of Nuclear Medicine, King Abdulaziz Medical City, Jeddah, Saudi Arabia
[c] King Saud Bin Abdulaziz University for Health Sciences, Jeddah, Saudi Arabia

ARTICLE INFO

Keywords:
GATE
Reconstruction
SPECT
Arms
Heart
Myocardial
Perfusion
STL

ABSTRACT

Arms influence in myocardial perfusion single photon emission computed tomography (SPECT) imaging has been studied for the last two decades. These studies suggested that arms positioning next to the patient would not show cardiac abnormalities or perfusion defects in SPECT imaging while it would not affect the scan during positron emission tomography (PET) scans. As a recent improvement in Geant4 Application for Tomographic Emission (GATE), -a Monte Carlo simulation toolkit- a new feature was added to enable the use of STereoLithography (STL). STL files are implanted as an input geometry for most human organs, which would give superior advantages in details compared to analytical geometry shapes. This study is adopting this recent improvement in GATE to study arms effect in SPECT imaging with the consideration of four scenarios; normal heart perfusion imaging with and without arms positioned next to the patient and two of the same scenarios with a perfusion myocardial defected. The results showed that perfusion defect could be observed with arms next to the patient. For image reconstruction, both filtered backprojection (FBP) and iterative technique – maximum likelihood expectation maximization (MLEM) were used. The MLEM was performed to analyse the four different patient scenarios. The difference in counts between arms-up and arms-down position for the abnormal case was shown to be less than 6%. The conclusion from this paper is that arm influence during abnormal heart SPECT imaging can be measured and has a minimal contribution to the reconstructed images.

Introduction

Single photon emission computed tomography (SPECT) scans for myocardial perfusion require that patients are to position their arms above their head. This “arms-up” positioning was believed to be necessary to avoid the beam being attenuated from both sides by the arms. The positioning of the arms next to the thorax also known as “arms-down” position could reduce the counts [1]. Consequently, this may cause some regions in the image to exhibit lower activity. This reduction in activity might cause a reduction in resolution or degradation to the image quality which may lead to misdiagnosis [1]. The attenuation correction is expected to facilitate the significant reduction of the artifacts observed at arms-down position by applying the appropriate correction factor to compensate for the sensitivity losses at projection angles where the arms are located between the scanned area of the subject and the SPECT detector heads. However, the noise elevation due to the loss in sensitivity at those angles will remain.

Compared to SPECT, PET typically uses higher photon energy; therefore, arms positioning is not a major concern in PET myocardial studies. In fact, during PET scans, some studies were carried out with patient arms positioned down.

The arms-up position is considered uncomfortable and, in many cases, painful [2]. Keeping in mind the patient’s age and that some scans take about 30–40 min, it might be difficult to maintain that position in most cases. Furthermore, patient discomfort induces motion which increases the likelihood of motion artifacts [3,4].

Many researchers were motivated to find an alternative technique that preserves the image quality and provides less patient discomfort. Multiple studies in recent years suggested that arms-down position does not have any significant effect on image quality. Toma et al., showed through scanning 41 patients that arms positioning have no influence on image quality, abnormality location and extent [5]. Izaki et al., studied the two arms positions among normal and abnormal patients. No significant difference was observed in images produced of normal

* Corresponding author.
E-mail address: ebanoqitah@kau.edu.sa (E. Banoqitah).

https://doi.org/10.1016/j.rinp.2018.06.028
Received 21 November 2017; Received in revised form 27 May 2018; Accepted 14 June 2018
Available online 18 June 2018

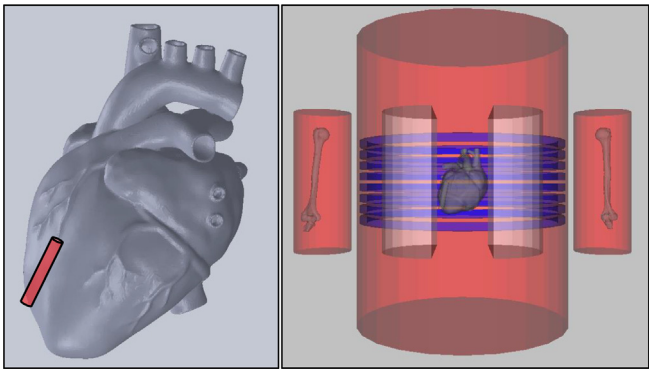

Fig. 1. (a) The heart STL used in simulation and a red cylinder representing the abnormality. (b) The full phantom used in the simulation. (For interpretation of the references to color in this figure legend, the reader is referred to the web version of this article.)

Table 1
GE discovery 670 collimator data.

Description	Crystal thickness (mm)	Type Of hole	Hole diameter (mm)	Septal thickness (mm)	Hole length (mm)	Energy resolution (keV)
Low Energy General Purpose (LEGP)	10	Hex	2.5	0.4	40	140 ± 15%

cases. However, the study reported that the arms-down position could lead to underestimation of abnormality among abnormal patients which could lead to misdiagnosis [3]. Furthermore, some studies suggested that non-uniformity that was created by the arms could be reduced using transmission attenuation correction techniques [6,7]. Alternatively, acquisition time may be increased from angles affected to compensate for arm attenuation [1].

Several simulation packages can be used for studying arms positioning influence, including GATE. GATE was developed to deliver accurate tomographic emission simulation, which provides tools that facilitate the acquisition of tomographic data for SPECT studies. In addition, GATE 8 introduced the possibility of tessellated volume creation. Such volumes can be created through importing stereolithography "STL" files into the simulation. STL is one of the common file formats that are used for defining 3D models. This feature would allow more accurate mimicking of several geometrically complicated organs [8]. Alternatively, such organs can be accurately simulated by importing CT data into the simulation to generate a voxelized phantom. These digital phantoms require additional data to transform the CT data into material and volume definitions. Both STL and voxelized phantoms are superior to traditional analytical phantoms when it comes to organ modeling. The selection of geometry modeling method depends on the application. For example, it might be more convenient when mimicking a single complicated organ to use an STL file instead of CT data. The major advantage of using simulation lies in its capability in limiting the number of variables that affect the results, allowing each variable to be studied independently.

The simulation output generated for each scenario will be reconstructed into slices. The reconstruction process can be carried out using filtered backprojection "FBP" or iterative algorithms. Nuclear medicine uses much lower photon count rates to produce data compared to X-ray CT, resulting in more noisy data. Iterative reconstruction is more capable of coping with noise than filtered backprojection. Consequently, iterative reconstruction produces a higher signal to noise ratio (SNR) images and as a result, it is more popular in nuclear medicine [9]. In this study, both algorithms were considered.

The aim of this research is to study the influence of the arms-down position on the quality of the reconstructed image and the possibility of misdiagnosis. This study will be carried out through simulating the two arms positioning with and without the presence of perfusion defects.

Materials and methods

Phantom

The phantom developed within the simulation consists of a 30-cm diameter cylindrical resembling the human abdominal region that is composed of water with two smaller cylinders with 8 cm diameter composed of muscle where each represents one of the arms. The thorax cylinder contains a set of 8 rings simulating the ribcage, two air cylinders representing the lungs, and an STL 3D model of the heart as illustrated in Fig. 1. The arms' cylinders only contain an STL 3D model of the humerus that is surrounded by muscle tissue. The use of tessellated volumes lengthens the simulation time; therefore, the use of 3D models to simulate the lungs and the ribcage was avoided.

Both radioisotopes Tl-201 and Tc-99 m are usually used for myocardial studies [10]. The latter was preferred for its emission of lower energy photons (140 keV). Energy is significant since lower energy photons have a higher attenuation probability. The radioisotope was

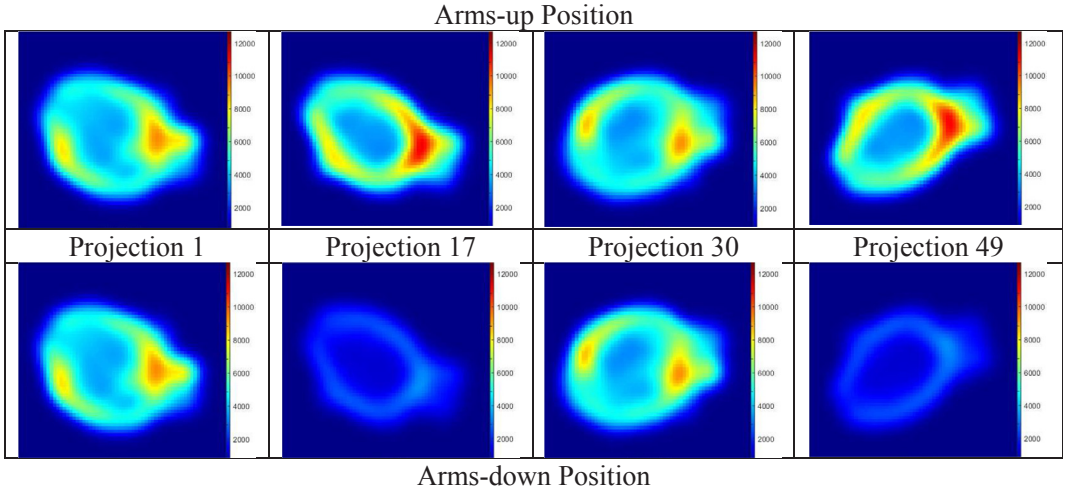

Fig. 2. Projections obtained from the simulation at angles where the arm position effect could be noticed.

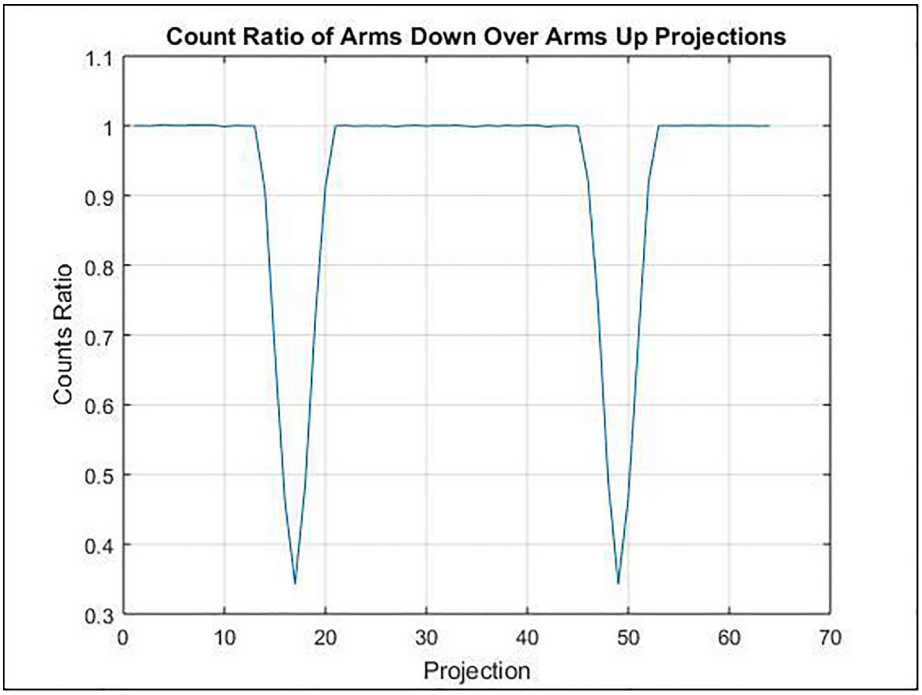

Fig. 3. The counts ratio of arms-down to arms-up position.

uniformly distributed within the heart tissue. An abnormality was added to one side of the heart through replacing part of the heart tissue by a vacuum, creating a defect in the heart volume.

SPECT system and acquisition parameters

The SPECT system used in the simulation was designed using an existing SPECT specification of collimator, crystal and energy resolution, see Table 1. The system consisted of four gamma cameras. The camera consisted of 12.5 × 12.5 cm NaI crystals. The camera sensitive area was made small to cover only the heart. The system rotated in a circular path covering 360 degrees. Image matrix used for each projection was 64 × 64. Therefore, 64 projections were needed to reconstruct an acceptable image [9].

Reconstruction

There are several open source software and toolkits available for image reconstruction that provides FBP and iterative reconstruction algorithms. For the parallel beam FBP reconstruction, the "iradon"

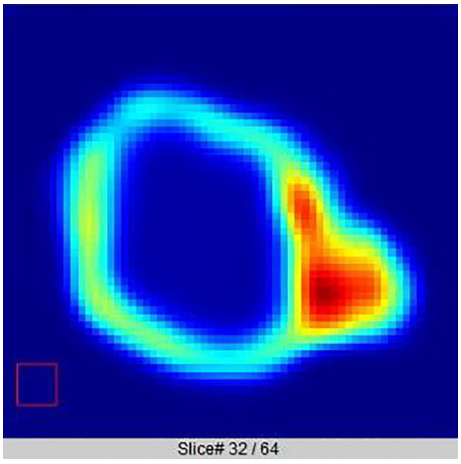

Fig. 5. ROI for averaging background signal in each iteration (ROI area marked with a red rectangle on the bottom left corner). (For interpretation of the references to color in this figure legend, the reader is referred to the web version of this article.)

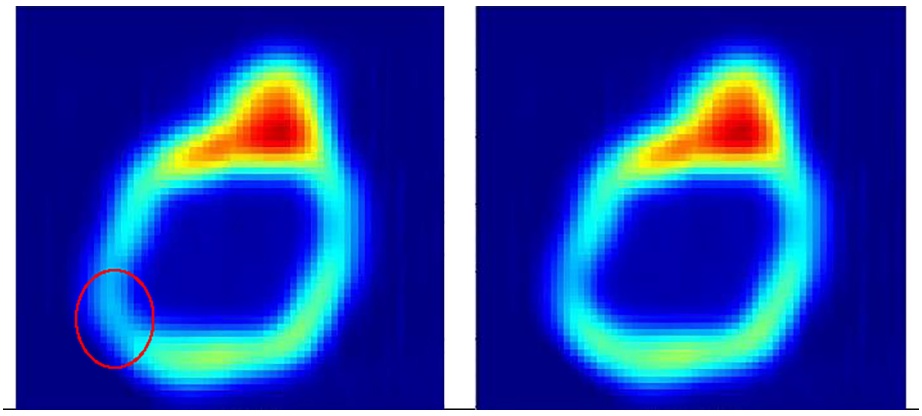

Fig. 4. The filtered back projection reconstructed slices on the left the data with the abnormality (marked with the red circle) and on the right the normal data set. (For interpretation of the references to color in this figure legend, the reader is referred to the web version of this article.)

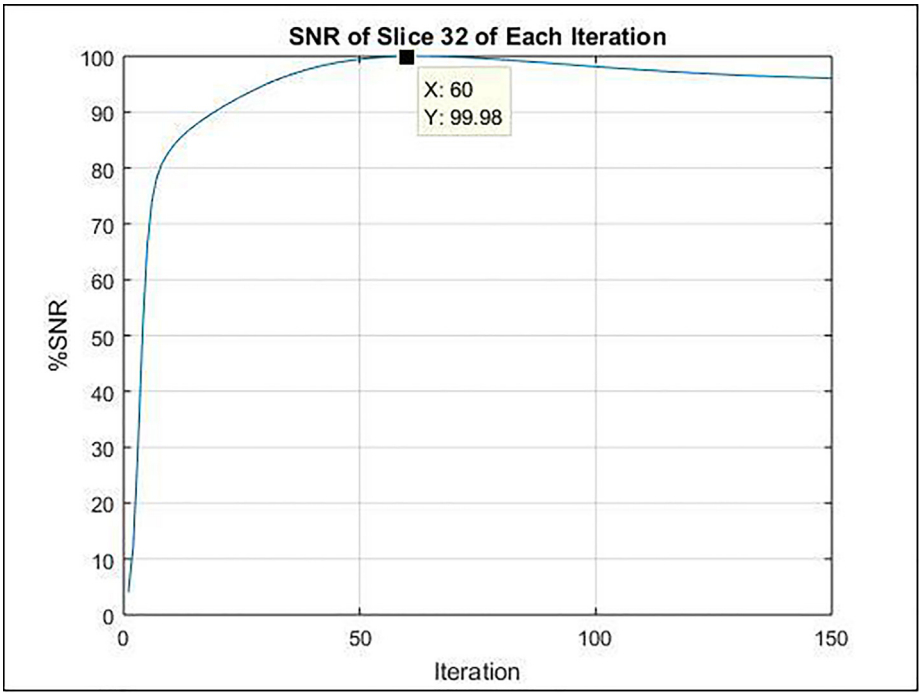

Fig. 6. SNR percentage over each iteration.

built-in function in MATLAB was used. The function basically reconstructs slices from sinograms obtained using parallel beam geometry. The "iradon" function had various types of frequency domain filters. Ramp filter with a cut-off frequency of 1 was used to reduce the star artifact.

As for iterative reconstruction, NiftyRec-2.3.2 was used. NiftyRec is a tomographic reconstruction toolkit with both MATLAB and python interfaces. It includes several iterative reconstruction algorithms such as MLEM, Ordered Subsets Expectation Maximization (OSEM) and One Step Late Maximum A Posteriori Expectation Maximization (OSL-MAPEM) [11].

Analysis

Projections can indicate how arms position can affect uniformity. This can be carried out through determining the count ratio of myocardial perfusion arms-down position to the arms-up position for every projection of the normal case. Although projections can give some indications, it is difficult to anticipate how any non-uniformity or artifact will be mapped into the reconstructed image.

Image quality in iterative reconstruction techniques depends on the number of iterations. Up to a certain number of iterations, resolution and SNR improve as the number of iterations increase. Beyond that number, resolution keeps improving but at the expense of increasing noise [12]. Therefore, the number of iterations selection depends on SNR. The reconstructed image with the highest SNR was compared to the image reconstructed using FBP technique. SNR was calculated as shown in Eq. (1):

$$SNR = \frac{x}{\bar{b}} \tag{1}$$

where x is the maximum signal value in the 32nd slice of each iteration and $\bar{b}$ is the background mean value of the same slice outside of the object as shown later in Fig. 5.

Furthermore, the SNR was compared between the two arm positions in the presence of an abnormality. From such comparison, one could

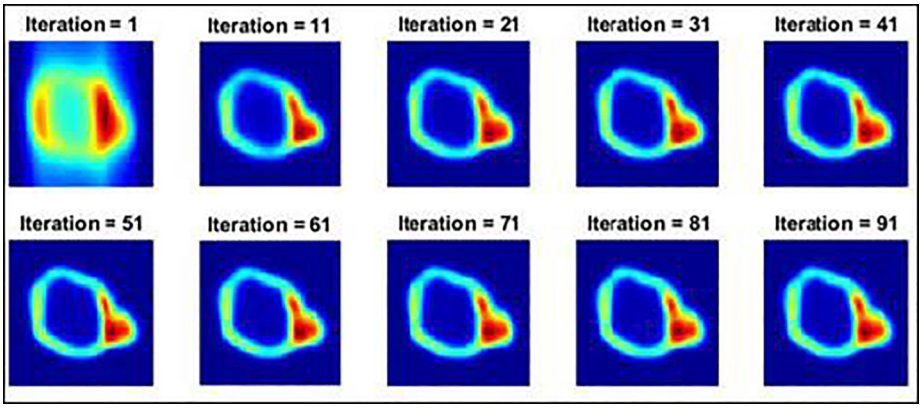

Fig. 7. Iteration samples of the abnormal data showing slice number 32.

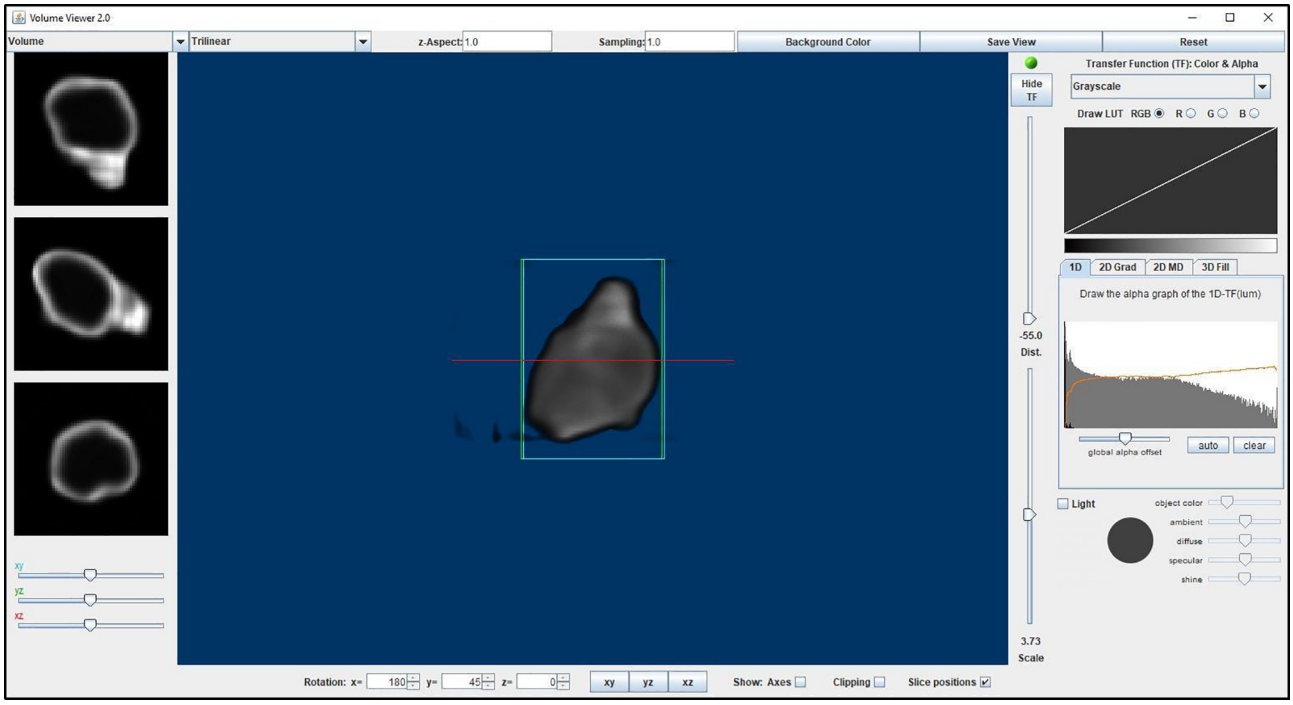

Fig. 8. The volumetric view of the heart after the reconstruction.

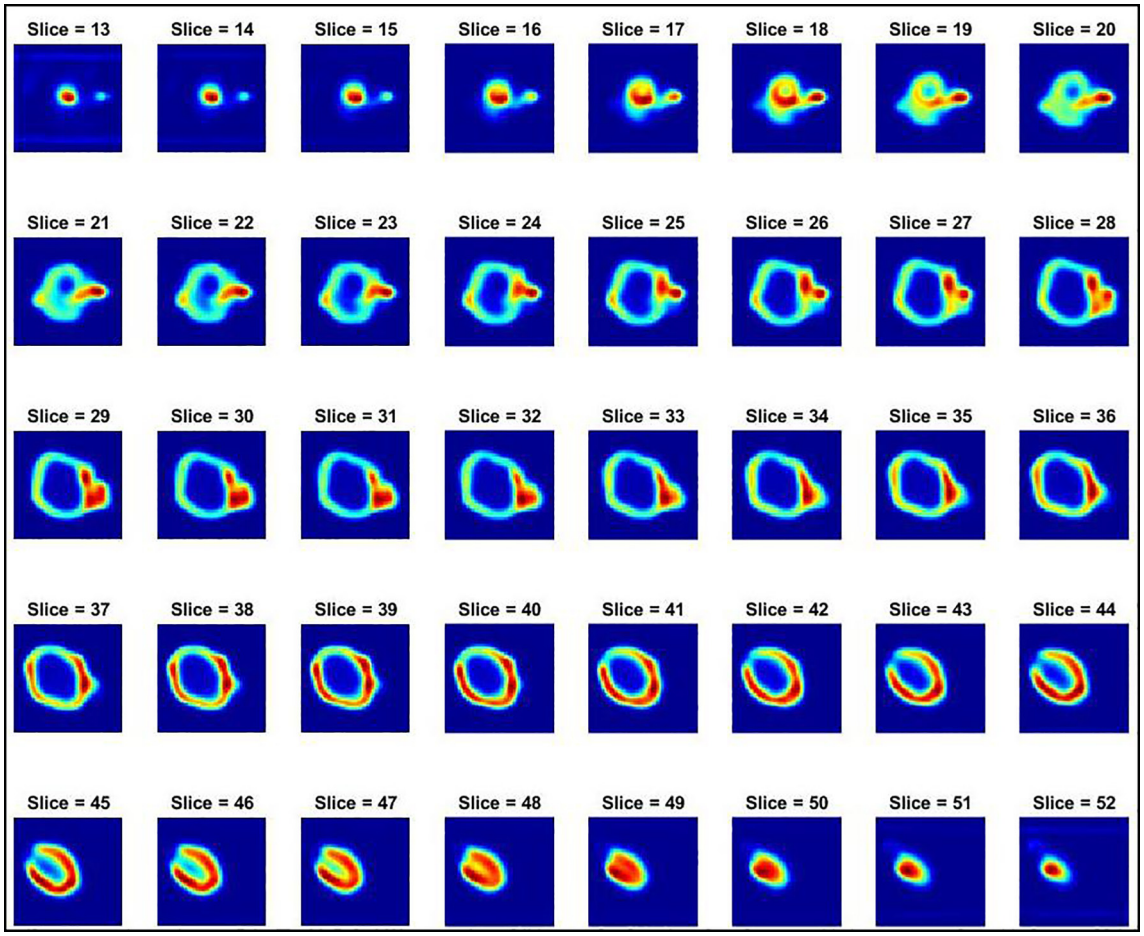

Fig. 9. The axial view of the reconstructed slices for the normal case with the arms-up position.

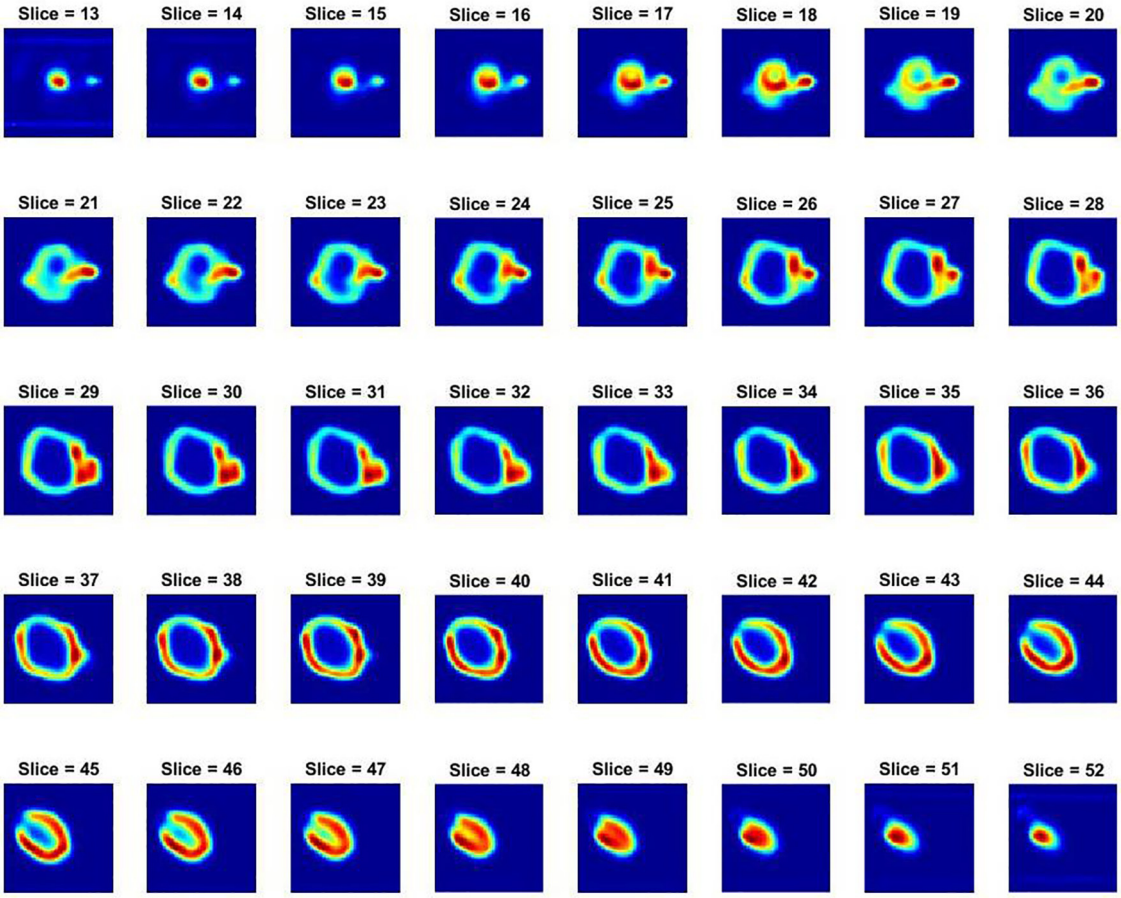

Fig. 10. The axial view of the reconstructed slices for the abnormal case with the arms-up position.

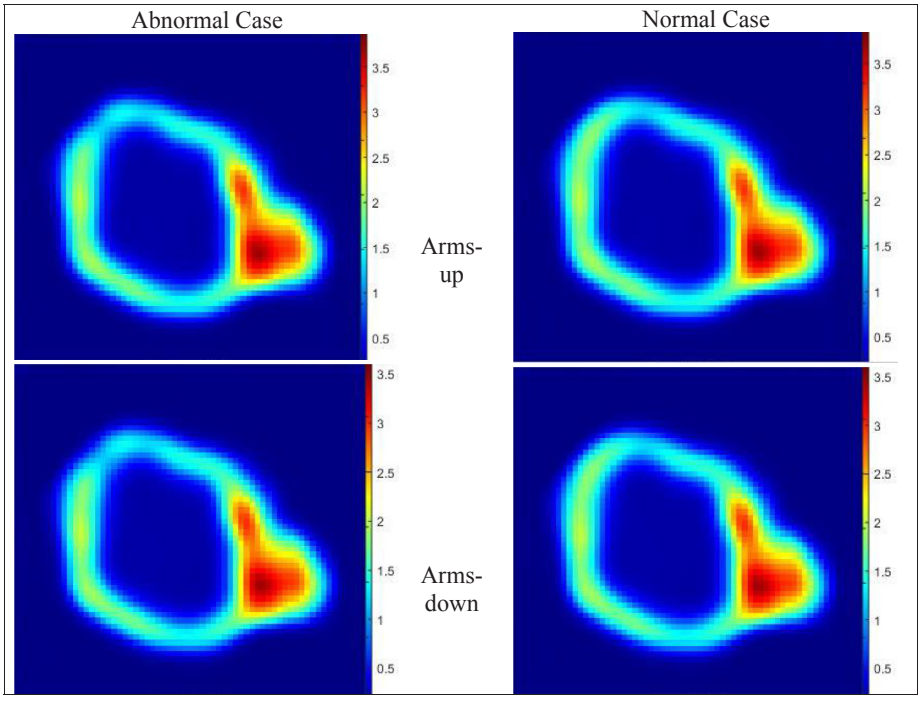

Fig. 11. Axial view of the four cases, abnormal on the left and normal on the right with arms-up in the upper row and arms-down in the lower row.

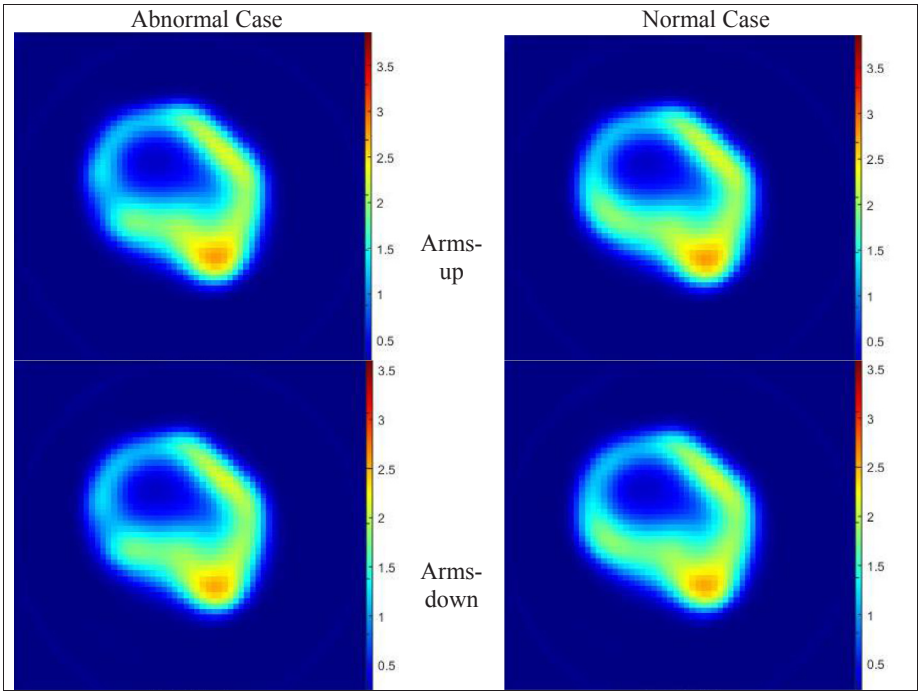

Fig. 12. Sagittal view of the four cases, abnormal on the left and normal on the right with arms-up in the upper row and arms-down in the lower row.

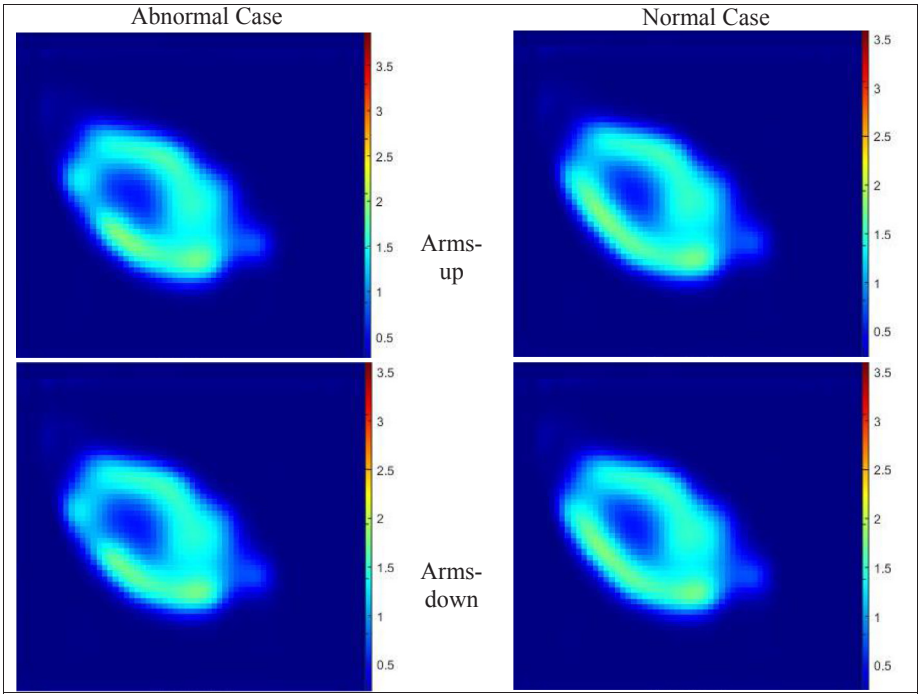

Fig. 13. Coronal view of the four cases, abnormal on the left and normal on the right with arms-up in the upper row and arms-down in the lower row.

deduce whether the arms-down position could cause abnormality underestimation. The extent of underestimation was figured out through abnormality size, location, and mean count.

Results

The obtained projections from the simulation were 64 with the size of 64 × 64 pixels for each scenario. Fig. 2 shows the normal case projections with the arms-up position. The SNR was above 100, which was more than what was needed to indicate the usefulness of the quality of the images. To see the effect of the arms on the projections, Fig. 3 shows the counts ratio of the arms-down to the arms-up position for the normal case. The effect of the arms presence was noticeable on the projections from projection 14–20 and again at 45–51.

When the images were run through the reconstruction code, the parallel beam reconstruction method, at first, was used on the arms-up projections for both the normal and abnormal cases using iradon as depicted in Fig. 4. The resulted output was noisy and with relatively low measured metric SNR at 43 and at some slices (first 5 and last 5 of the slices set) went down to 2. The abnormality was barely visible

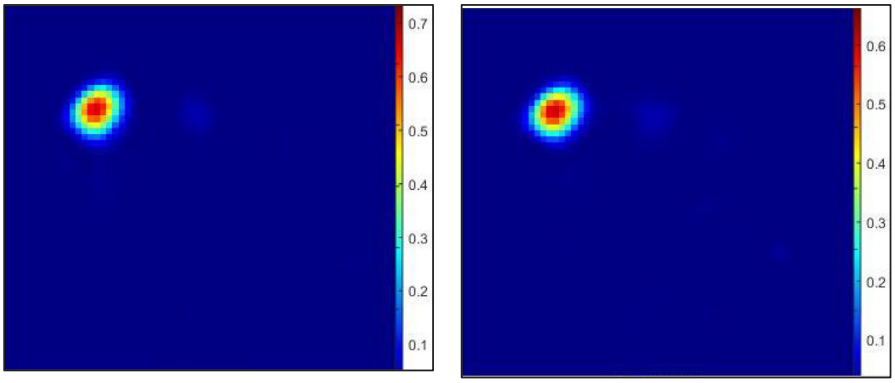

Fig. 14. Images obtained by subtracting the abnormal case images from the normal in (a) arms-up and (b) the arms-down positions.

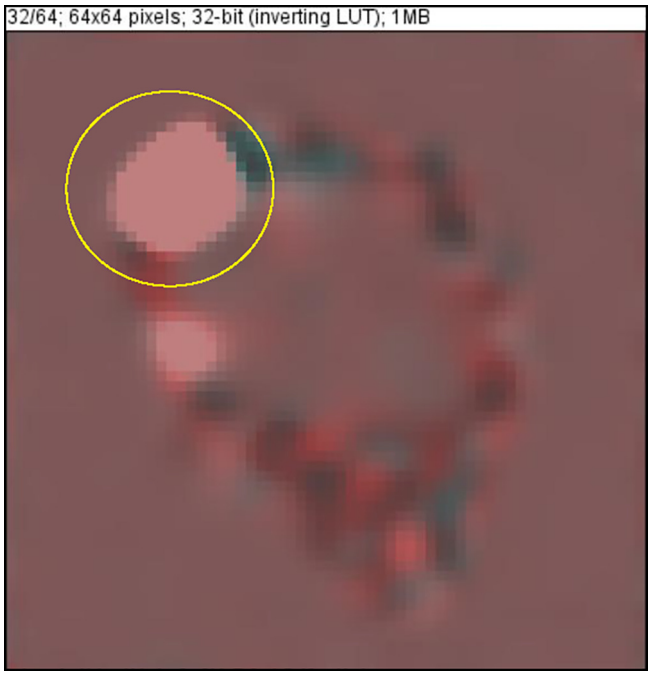

Fig. 15. The two abnormalities overlaid over each other: the white pixels represent the matching area.

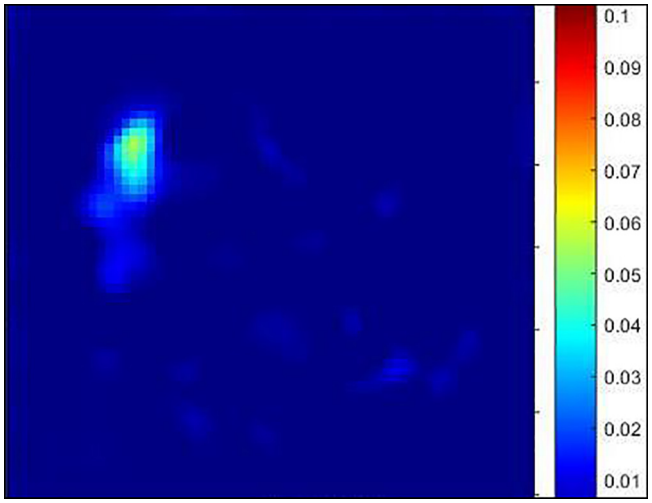

Fig. 16. Resulted area of subtracting "Fig. 14(a)" from "Fig. 14(b)".

making this reconstruction method not reliable.

Therefore, the MLEM iterative method was used through Nifty-2.3.2 toolkit as an alternative approach. Initially, the number of iterations needed to produce an acceptable reconstructed image had to be determined. Therefore, 60 iterations were used on the abnormal situation with the arms-up position. After generating the slices, the SNR was measured for each iteration at slice 32 (which is the mid-point) using MATLAB, see Fig. 5 below:

The SNR initially increases as the number of iterations increases until reaching iteration 50 as seen in Fig. 6. Beyond iteration 50, the SNR plateaus at first and then followed by a slight decrease in SNR as the number of iterations increase.

The suitable number of iterations was found to be between 50 and 75 iterations during the plateau, before the SNR drops as the number of iterations is increased. When visually examining slice 32 of the data in Fig. 7, the same outcome could easily be noticed when viewing samples of the iterations. Taking that into consideration, 60 iterations were chosen as the number of iterations used, where the SNR was about 140, the point is before the plateau and away from the edge of converging.

The resulted 3D object was generated from the reconstructed slices using ImageJ volume viewer slices (Fig. 8). The reconstructed 3D image shows a complete heart shape that can be viewed in three planar views.

After choosing the proper number of iterations, the projection data for each scenario was reconstructed into slices. The axial views of the reconstructed images for the arms-up normal and abnormal cases can be seen in (Figs. 9 and 10), respectively. The abnormality can be localized by comparing the two images sets. As a result, the abnormality (defect lesion) can be seen in slices 30–37. This was a significant result that allowed us to determine later which slices to examine, with respect to the abnormality, in the images reconstructed from SPECT data acquired at the arms-down position.

Fig. 11 shows a comparison of the 32nd reconstructed slice for all scenarios. The presented images were displayed with the same contrast window to provide an accurate visual assessment. Although the abnormality was observed in both the arms-up and down cases, the signal of the latter case was less by 6.5% on average. However, the minimum counts did change at some points which was understandable because of the increased scattered radiation the arms caused, this change was still less than 15.5%.

Moreover, to prove that the arms did not affect the detectability of the abnormality when they were placed on the side of the patient, another two views of the data set were shown in Fig. 12 showing the sagittal view and Fig. 13 showing the coronal view.

To compare abnormalities, images with abnormalities were subtracted from the normal case images. The resultant images, depicted in Fig. 14, represent the signal difference between the normal and abnormal cases. Since the same seed (the initial value used in Monte Carlo method) was used for all simulation experiments, any difference

between the images is caused by the abnormality. The signal difference was caused by the activity distribution difference. The same activity was used in all cases, but when the abnormality was added, the area shared with the heart did not emit any radiation. As a consequence, the activity was distributed over a smaller volume causing a difference in counts between the normal and abnormal cases. This difference in counts was less in the arms-down case for the arms remove some of the photons creating the difference. Therefore, aside from the abnormality area, the subtracted images showed a higher mean signal in the case of the arms-up position, compared to the arms-down position.

The difference in the abnormality size could be estimated by studying if the arms presence had an impact on the detected size of the abnormality as what the previous study predicted [3]. Using ImageJ, by overlaying image “a” over image “b” from Fig. 14 one could compare their sizes where “a” is represented in cyan and “b” in red as shown in Fig. 15. The resulted white color area of the image is the result of overlapping red with cyan color regions. If the counts in the red image were higher (in the order of thousands compared to the cyan image) the resulted image would be red. However, when both the images have the same number, the resulted area would be white. Fig. 15 shows that the arms-down abnormality to be exactly matching with the arms-up abnormality case in size. Moreover, Fig. 16 shows the resulted area of subtracting “Fig. 14(a)” from “Fig. 14(b)” which matched the area of the abnormality used in the simulation. When studying, the values closely, the absolute mean difference of the entire image value was 0.001 (less than 0.015%). This means that the difference seen is believed to be caused by scattered radiation from the arms when they are present. This value is small to not have any significant effect on the results.

Study limitations

This study represented a design similar to a commercial SPECT system to image the myocardial perfusion. The use of a clinical SPECT system with the absence of attenuation map would show a limitation while many clinics still do not have a CT-scan or hybrid system to make a correction for the system counts. The images acquired and reconstructed represented the amount of deterioration in the image caused by the arms presence and the governing by the gamma camera system design as illustrated in Table 1.

This study considers a single possible scenario. It does not provide much information on how changing patient size, abnormality size, changing radioactive source, or the imaging system specifications would affect the outcome of the study.

Conclusion

Our study has demonstrated that the new feature of STL implantation into GATE as a geometry input file can be very useful to create a realistic representation of the normal and abnormal myocardial activity distribution in PET and SPECT simulation studies. However, further clinical SPECT imaging studies are required to validate, against real human myocardial perfusion SPECT data.

From the results obtained, it was noted that it is possible to rely on GATE to investigate the effect of arms positioning using STL geometry and to use MATLAB to reconstruct the data. In addition, it was clear that having the arms-down position instead of the arms-up had an effect with less than 6% which did not significantly affect the data obtained and abnormalities were still visible even with reduced counts. Further investigation will be carried out using a commercial system and then compared to the results with experimental data.

Appendix A. Supplementary data

Supplementary data associated with this article can be found, in the online version, at http://dx.doi.org/10.1016/j.rinp.2018.06.028.

References

[1] Luo Dershan, King MA, Pan Tin-Su, Xia Weishi. Evaluation of the effects of patient arm attenuation in SPECT cardiac perfusion imaging. IEEE Trans Nucl Sci 1996;43:3291–9. http://dx.doi.org/10.1109/23.552738.
[2] Fricke H, Fricke E, Weise R, Kammeier A, Lindner O, Burchert W. A method to remove artifacts in attenuation-corrected myocardial perfusion SPECT Introduced by misalignment between emission scan and CT-derived attenuation maps. J Nucl Med 2004;45:1619–25. 0161-5505.
[3] Izaki M, Soares Junior J, Giorgi MCP, Meneghetti JC. Influence of the arm position in myocardial perfusion imaging acquisition. Rev Assoc Med Bras 2014;60:311–7. http://dx.doi.org/10.1590/1806-9282.60.04.009.
[4] Botvinick EH, Zhu YY, O'Connell WJ, Dae MW. A quantitative assessment of patient motion and its effect on myocardial perfusion SPECT images. J Nucl Med 1993;34:303–10.
[5] Toma DM, White MP, Mann A, Phillips JM, Pelchat DA, Giri S, et al. Influence of arm positioning on rest/stress technetium-99m labeled sestamibi tomographic myocardial perfusion imaging. J Nucl Cardiol 1999;6:163–8. http://dx.doi.org/10.1016/S1071-3581(99)90076-4.
[6] Araujo LI, Jimenez-Hoyuela JM, McClellan JR, Lin E, Viggiano J, Alavi A. Improved uniformity in tomographic myocardial perfusion imaging with attenuation correction and enhanced acquisition and processing. J Nucl Med 2000;41:1139–44.
[7] Prvulovich EM, Jarritt PH, Lonn AHR, Vorontsova E, Bomanji JB, Ell PJ. Influence of arm positioning on tomographic thallium-201 myocardial perfusion imaging and the effect of attenuation correction. Eur J Nucl Med 2000;27:1349–55. http://dx.doi.org/10.1007/s002590000288.
[8] Jan S, Santin G, Strul D, Staelens S, Assié K, Autret D, et al. GATE: a simulation toolkit for PET and SPECT. Phys Med Biol 2004;49:4543–61. http://dx.doi.org/10.1088/0031-9155/49/19/007.
[9] Bushberg JT, Seibert JA, Leidholdt EM, Boone JM, Goldschmidt EJ. The essential physics of medical imaging. vol. 30. 3rd ed. 2012. doi:10.1118/1.1585033.
[10] Henzlova MJ, Duvall WL, Einstein AJ, Travin MI, Verberne HJ. ASNC imaging guidelines for SPECT nuclear cardiology procedures: Stress, protocols, and tracers. J Nucl Cardiol 2016;23:606–39. http://dx.doi.org/10.1007/s12350-015-0387-x.
[11] NiftyRec 2.0 n.d. http://niftyrec.scienceontheweb.net/ [accessed 30.09.2017].
[12] Powsner RA, Powsner ER. Essential nuclear medicine physics. Malden Massachusetts, USA: Blackwell Publishing, Inc.; 2006. http://dx.doi.org/10.1002/9780470752890.